ACS APPLIED MATERIALS & INTERFACES

Research Article

www.acsami.org

Quantum Dot and Superparamagnetic Nanoparticle Interaction with Pathogenic Fungi: Internalization and Toxicity Profile

Nicolas Rispail,[†] Laura De Matteis,[‡] Raquel Santos,[§] Ana S. Miguel,[§] Laura Custardoy,[∥] Pilar S. Testillano,[⊥] María C. Risueño,[⊥] Alejandro Pérez-de-Luque,[#] Christopher Maycock,[§,△] Pedro Fevereiro,[§,△] Abel Oliva,[§] Rodrigo Fernández-Pacheco,[∥] M. Ricardo Ibarra,[‡,∥,□] Jesús M. de la Fuente,[‡,¶] Clara Marquina,[□,○] Diego Rubiales,[†] and Elena Prats*[,†]

[†]Instituto de Agricultura Sostenible, CSIC, Alameda del Obispo s/n, Córdoba, Spain

[‡]Instituto de Nanociencia de Aragón, Universidad de Zaragoza, C/Mariano Esquillor s/n, Zaragoza, Spain

[§]Instituto de Tecnologia Química e Biológica, Universidade Nova de Lisboa, 2780-157 Oeiras, Portugal

[∥]Laboratorio de Microscopías Avanzadas (LMA), Instituto de Nanociencia de Aragón (INA), Universidad de Zaragoza, Zaragoza, Spain

[⊥]Centro de Investigaciones Biológicas-CSIC, Ramiro de Maeztu 9, 28040 Madrid, Spain

[#]IFAPA, Centro Alameda del Obispo, Avenida Menéndez Pidal s/n, Córdoba, Spain

[¶]Fundación ARAID, 50018 Zaragoza, Spain

[□]Departamento de Física de la Materia Condensada, Universidad de Zaragoza, Pedro Cerbuna 12, Zaragoza, Spain

[○]Instituto de Ciencia de Materiales de Aragón (ICMA), CSIC-Universidad de Zaragoza, Pedro Cerbuna 12, Zaragoza, Spain

[△]Faculdade de Ciências, Universidade de Lisboa, 1749-016 Lisbon, Portugal

Supporting Information

ABSTRACT: For several years now, nanoscaled materials have been implemented in biotechnological applications related to animal (in particular human) cells and related pathologies. However, the use of nanomaterials in plant biology is far less widespread, although their application in this field could lead to the future development of plant biotechnology applications. For any practical use, it is crucial to elucidate the relationship between the nanomaterials and the target cells. In this work we have evaluated the behavior of two types of nanomaterials, quantum dots and superparamagnetic nanoparticles, on *Fusarium oxysporum,* a fungal species that infects an enormous range of crops causing important economic losses and is also an opportunistic human pathogen. Our results indicated that both nanomaterials rapidly interacted with the fungal hypha labeling the presence of the pathogenic fungus, although they showed differential behavior with respect to internalization. Thus, whereas magnetic nanoparticles appeared to be on the cell surface, quantum dots were significantly taken up by the fungal hyphae showing their potential for the development of novel control approaches of *F. oxysporum* and related pathogenic fungi following appropriate functionalization. In addition, the fungal germination and growth, accumulation of ROS, indicative of cell stress, and fungal viability have been evaluated at different nanomaterial concentrations showing the low toxicity of both types of nanomaterials to the fungus. This work represents the first study on the behavior of quantum dots and superparamagnetic particles on fungal cells, and constitutes the first and essential step to address the feasibility of new nanotechnology-based systems for early detection and eventual control of pathogenic fungi.

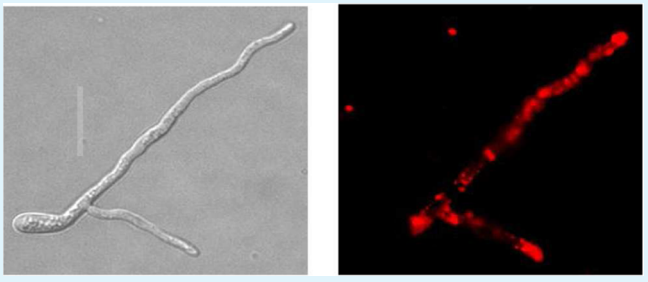

KEYWORDS: *superparamagnetic nanoparticles, quatum dots, Fusarium oxysporum, disease control, plant pathogens, toxicity*

1. INTRODUCTION

Members of the *Fusarium oxysporum* complex are well-known soilborne plant pathogens responsible for economically devastating vascular wilts of an enormous range of agronomically important plant hosts.[1] In addition, this fungus is an opportunistic pathogen of immunocompromised patients[2] that during deeply invasive infections of persistently neutropenic individuals causes 100% mortality. From an agronomical point of view, no completely effective treatments are available for this pathogen or related soil borne pathogens. The only effective

Received: February 19, 2014
Accepted: May 22, 2014
Published: May 22, 2014

control measure is soil sterilization, which is too costly for most farmers. Some control is achieved with fungicides. However, once wilt symptoms appear it is usually too late to apply an effective treatment[3] and, indiscriminate application of these fungicides leaves problematic residues both in the soil and fruit tissues.[4] Methods based on polymerase chain reactions have been developed to detect the fungus.[5] However, these are not ready to use in the field, are costly and require a relatively large amount of the fungus, indicative of advanced infection, to be detected. Thus, new highly sensitive methods for the early detection and/or effective control of this disease are required.

Recent decades have witnessed considerable research interest in the potential applications of nanoscaled materials in biological systems and despite having several advantages, they also have limitations. Their use in biological applications strongly depends on their possible cytotoxicity and on their transport through biological membranes and, in the case of fungi, also through the cell wall. Of the many nanoparticulated materials developed over the last 20 years, inorganic nanoparticles have been used for many applications.[6,7] A wide range of inorganic nanoparticles have been prepared and include noble metals, magnetic materials, and semiconductor nanocrystals, which, because of their size (typically in the range between 1 and 200 nm), have physical properties of interest for the development of novel sensing and diagnostic tools, as well as innovative therapeutic strategies.[6,8,9] Semiconductor nanocrystals, or quantum dots (QDs), are typically composed of a cadmium selenide (CdSe) core and a zinc sulfide (ZnS) shell. The wide adoption of QDs as imaging tools in biology and medical research stems from the fact that they readily penetrate cells without losing their unique photophysical properties, such as superior photoemission and high photostability.[10,11] Among magnetic nanoparticles (MNPs), magnetic iron oxide nanoparticles are widely used. These structures are biocompatible, and by tailoring their size, their magnetic behavior can be varied from ferrimagnetic to superparamagnetic, thereby making them suitable for an ample range of biomedical and biotechnological applications, such as contrast agents for magnetic resonance imaging and the magnetically targeted delivery of bioactive molecules,[12,13] as magnetic labels in biosensors[14] and as nanosorbents and photocatalysts in environmental cleanup technologies.[15,16] The above-mentioned characterisitics make both QDs and MNPs promising tools for novel applications in plant biology and plant biotechnology, similar to those already developed in the field of biomedicine.

To address the potential of QDs and MNPs for the future development of new and more effective strategies to fight against this pathogen, we studied the interaction between these nanomaterials and the *F. oxysporum* cells. We evaluated their internalization (paying special attention to the fungal cell wall) and toxicity on *F. oxysporum* cells, at different concentrations. From an agronomical point of view, in-depth knowledge of the behavior of the fungus in the presence of the nanomaterials is crucial to outline the toxicity profile of these particles. This is particularly relevant in the case of *F. oxysporum*, since in addition to other beneficial fungal spp. present in the rhizosphere, specific nonpathogenic *F. oxysporum* strains have been reported to cohabit with the pathogenic strains exerting biological control.[17] In order to improve the stability of these inorganic nanomaterials in biological suspensions, QDs were coated with 3-mercaptopropionic acid (MPA-QDs) and MNPs with aminated silica[18] (SiO_2-MNPs). Fluorescently labeled G proteins were also used to decorate the surface of the MNPs as a hook for future functionalization for further research purposes. For future detection and control purposes, out of the scope of this paper, the appropriate nanosized materials will have to be functionalized with the suitable biomolecule able to selectively target the pathogenic *formae speciales*, but only after internalization and toxicity studies, such as the presented in this work. Because fungal cells show commonalities in composition and structure, the methodology presented here could be relatively easily extrapolated to other phytopathogenic fungi.

2. EXPERIMENTAL SECTION

2.1. Fungal Isolates and Culture Conditions. *F. oxysporum* f.sp. *lycopersici* (*Fol*) race 2 wild type strain 4287 (FGSC 9935) was used in all the experiments. The fungal strain was stored as microconidial suspensions in 30% glycerol at −80 °C. For microconidia production, cultures were grown in potato dextrose broth (PDB; Difco, Detroit, MI) at 28 °C with shaking at 170 rpm.[19] To evaluate the potential toxicity of both nanomaterials, we grew 5×10^6 microconidia for 16 h at 28 °C under agitation at 170 rpm in 1 mL of liquid minimum medium (MM)[20] supplemented with either MPA-QDs at a concentration of 10, 50, 100, or 500 nM or SiO_2-MNPs at 25, 50, 100, and 500 $\mu g\ mL^{-1}$. To monitor their internalization, 5×10^6 microconidia were grown for 16 h at 28 °C under agitation at 170 rpm in 1 mL of liquid MM. For long-term internalization studies, the MPA-QDs and the SiO_2-MNPs were added at the time of *Fol* inoculation, whereas for short-term internalization, they were added to the MM after 16 h of growth and incubated for a further 10 min or 3 h before visualization.

2.2. Nanomaterial Synthesis. *CdSe/ZnS Core−Shell QDs.* All chemicals were obtained from Sigma-Aldrich, unless otherwise indicated, and used as received. UV−vis absorbance spectra were taken using a Beckman DU-70. Photoluminescence spectra were recorded with a SPEX Fluorolog spectrofluorimeter. TOPO/HDA-capped CdSe nanocrystals were synthesized using standard procedures as previously described.[21,22] Briefly, CdSe nanocrystals with the first absorption peak around 580−590 nm and a diameter of 3.6−4.5 nm were first generated and then passivated with 5 monolayers of ZnS. Passivation was achieved using the SILAR method,[23] which consists of alternating injections of Zn and S precursors into the solution containing the CdSe-core nanocrystals suspended in octadecene/hexadecylamine. After extraction with methanol, centrifugation and decantation, the particles were dispersed in chloroform for further processing. The mercaptopropanoic acid-QDs were obtained by the phase transfer method, as described previously.[21] The resulting hydrophilic QDs with an hydrodynamic diameter of 13.5 nm were then purified and concentrated using a Sartorius Vivaspin 6 tube (cutoff 10 kDa) at 7500 g.

The hydrodynamic diameter (HD) and zeta potential were measured by Dynamic Light Scattering (DLS) analysis using a Zetasizer Nano ZS dynamic light scatterer from Malvern Instruments. The HD was obtained from number-weighted size distribution analysis and reported as the mean of triplicate measurements. Zeta potential was measured only for hydrophilic QDs, because synthetic CdSe/ZnS QDs have little or no charge density on their surface and values were also reported as the average of triplicate measurements consisting of 20 runs each at 25 °C. The procedure was performed according to Miguel et al.[21] The obtained data were analyzed using the instrument's software (Zetasizer software, version 6.2). (For additional details of the characterization see Miguel et al.[21] and Figure S1 and S2 in Supporting Information).

SiO_2-MNPs. This type of nanoparticles was synthesized and characterized following De Matteis et al.[24] The particles were subsequently functionalized with an aminated silica coating and biofunctionalized by G protein adsorption on the aminated surface using the protocols reported in Arenal et al.[25] As mentioned in Arenal et al.[25] the size of the synthesized nanoparticles was between 100 and 150 nm (see the Supporting Information, Figure S3). To visualize the SiO_2-MNPs and to study their internalization in *F. oxysporum* hyphae,

an AlexaFluor488-conjugated G protein was also used to functionalize the nanoparticle surface.

2.3. Imaging MPA-QDs and the SiO_2-MNPs Interaction with Fungal Cells. To monitor the internalization of the MPA-QDs and the SiO_2-MNPs by fungal cells, samples were visualized after 10 min and 3 and 16 h of incubation with either 100 nM of MPA-QDs or 200 μg mL^{-1} of SiO_2-MNPs using Confocal, Transmission Electron Microscopy (TEM) and Energy-Dispersive X-ray Spectra (EDS) microscopy. In addition, to monitor their eventual exit from the fungal cells, 16-h-old conidial suspensions incubated with each type of nanomaterial were passed through a 0.45 μm filter (Whatman) to remove all unbound MPA-QDs and SiO_2-MNPs, and the mycelium was resuspended in sterile MM and incubated for an additional 4 h at 28 °C.

Confocal images were acquired in an AxioImager M2 microscope equipped with the objectives ECPlan-Neofluor x63/1.25 oil, (Carl Zeiss Microimaging, Germany) and appropriate filters (Texas Red ex595/em620; FITC ex490/em525 and DIC with Normasky) and a cooled charge-coupled device camera Photometrics Evolve (Photometrics, Tucson, AZ) with AxioVision 40 v4.8.2.0 Hotfix 09-PV CamEvolve software. Thin time-course confocal optical sections (~1 μm thick) were acquired using <20% laser intensity and operating in the mode 1024 × 1024, 400 Hz (~1/2 s per frame). For quantification purposes, gain and offset settings were kept constant so that the average background pixel intensity was between 0 and 10 and the fluorescent signal emitted by the cells was between 60 and 220 (0−255 scale for 8 bit images).

The interaction of the fungal cells with the SiO_2-MNPs was studied by cryo-TEM techniques in a Tecnai F30 (FEI), operated at 300 kV. In order to avoid damaging the samples by exposure to high vacuum in the microscope column, samples were vitrified in liquid ethane with an FEI Vitrobot, transferred to a Gatan cryo-holder, and then kept at liquid nitrogen temperature during the measurement. During vitrification, a thin amorphous layer of ice is formed, which protects the sample and preserves it in its original state in aqueous suspension. To identify the presence of the particles and also to discard any significant changes in morphology or size of the fungal cells, samples were observed in TEM mode.

In Scanning-Transmission Electron Microscopy (STEM) mode, a narrow probe is formed and the sample is scanned. Electrons scattered at high angles were collected with a High Angle Annular Dark Field detector to obtain Z-contrast images. Focal series of STEM-HAADF images were acquired so as to locate individual particles inside the fungal cells. Energy-Dispersive X-ray Spectra (EDS) were also obtained with an EDAX detector to assess the interaction of the magnetic particles with the cells and to identify their chemical composition.

2.4. Magnetic Separation Assays and Turbidity Measurements. Taking advantage of the magnetic properties of the SiO_2-MNPs, we performed magnetic separation assays to further study the interaction of these particles with *F. oxysporum* cells. For this purpose, two separate experiments were carried out.

In the first (long-incubation), conidial suspensions were incubated with or without a 200 μg mL^{-1} solution of SiO_2-MNPs for 16 h. The suspensions were then filtered to remove nanoparticles not internalized/attached (in)to the fungal mycelium, and the mycelium was resuspended in new fresh medium. This new suspension was placed in a well of a magnetic separation rack (MagnetoPURE-Micro, X-Zell), in which the magnets are placed on the lateral surface of the well. The suspension was kept under the magnetic field for 1, 3, and 5 min. At these times, an aliquot of the medium was taken, and the turbidity, indicative of mycelium concentration, was recorded spectrophotometrically at 600 nm (A_{600}). The reduction in absorbance with respect to a similar aliquot taken in the absence of the magnet (control) was recorded as indicative of the nanoparticle internalization/attachment (in)to the fungus and therefore of its attraction by the magnet. Three replicates per treatment were done. In a second experiment (short-incubation), a conidial suspension grown for 16 h in the absence of SiO_2-MNPs was subsequently incubated with or without the nanoparticles for 5 and 15 and 30 min, filtered, resuspended, and introduced into the magnetic separation rack. Aliquots of the medium were then taken and measured as described above.

2.5. Assessment of MPA-QDs and SiO_2-MNPs Toxicity on *F. oxysporum* Cells. *Colony Growth Assessment.* From each preparation, various parameters relative to colony growth, such as percentage of germination, percentage of long and small hyphae, and average area of hyphae were microscopically assessed. Long hyphae were considered to be those more than 2-fold the length of the conidia. Assessment of average area of hyphae was performed on the micrographs with the help of ImageJ free-software.

Reactive Oxygen Species (ROS) Accumulation and Oxidative Stress Assessment. ROS formation in fungal cells exposed to the different nanomaterials and concentrations was evaluated using three probes: 3,3′-diaminobenzidine (DAB) and nitroblue tetrazolium (NBT), which are specific to hydrogen peroxide (H_2O_2) and superoxide anion ($O_2^{-\bullet}$) respectively, and 2′,7′- Dichlorodihydrofluorescein diacetate (H_2DCFDA), which is a nonspecific probe for ROS accumulation. Two controls were prepared for each experiment. A negative control was used, which consisted of fungal conidia placed in the same conditions as the assay but without the addition of MPA-QDs and SiO_2-MNPs. As a positive control, cells were heated at 50 °C for 20 min and immediately cooled on ice for 2 min. All experiments were carried out in triplicate.

1. H_2O_2 Detection. The production of H_2O_2 at the cellular level was examined by applying the 3,3′-diaminobenzidine (DAB) staining technique described by Thordal-Christensen et al.[26] with a few modifications. DAB reacts rapidly with H_2O_2 in the presence of peroxidase, forming a brown polymerized product. For this purpose, a 200 μL aliquot of each 16 h old cell suspension culture of *F. oxysporum* was transferred to a sterile 1.5 mL Eppendorf tube and supplemented with 1 mM of DAB. All samples were then incubated in an orbital shaker at 170 rpm, in the dark, at 28 °C for 90 min before observation under a bright-field microscope.

2. $O_2^{-\bullet}$ Detection. $O_2^{-\bullet}$ was detected as described by Fryer et al.[27] with slight modifications, and similarly to the DAB assay. Nitro-substituted aromatics such as NBT can be reduced by $O_2^{-\bullet}$ to the monoformazan (NBT^+), with the accumulation of dark spots of blue formazan. For this purpose, a 200 μL aliquot of each 16 h old cell suspension culture of *F. oxysporum* was transferred to a sterile 1.5 mL Eppendorf tube and supplemented with 0.5 mM NBT. All samples were then incubated in an orbital shaker at 170 rpm, in the dark, at 28 °C for 4 h before observation under a bright-field microscope.

3. Cellular Oxidative Stress Assay. The cell-permeant 2′,7′-dichlorodihydrofluorescein diacetate (H_2DCFDA) reagent was used to determine cellular oxidative stress, as described by Ortega-Villasante et al.[28] using the same procedure as for the previous assay, but adding 20 μM of H_2DCFDA instead of NBT or DAB. After 90 min of incubation in the dark at 28 °C under agitation at 170 rpm, samples were visualized under a UV light microscope (ex = 488 and em = 525 nm). At least 35 germlings were assessed from each preparation, measuring the fluorescein intensity with ImageJ software as previously described.[29]

Fungal Cell Viability. Cell viability was assessed through the Evans Blue stain assay.[30] A diluted solution of Evans Blue (0.25% final concentration) was freshly prepared at the time of the assay, adding 10 μL of the 5% stock solution to a 200-μL aliquot of fungal suspension. A drop of 10 μL of the conidial suspension incubated with MPA-QDs and SiO_2-MNPs was then placed on a microscope slide. The counts were performed using a visible light microscope. As a positive control, cells were heated either at 90 °C for 5 min or at 50 °C for 20 min. In both cases, cells were then cooled on ice for 2 min before Evans Blue staining.

2.6. Statistical Analysis. All experiments followed a randomized design. For ease of understanding, means of raw percentage data are presented in the tables and figures. However, for statistical analysis, data recorded as percentages were transformed to arcsine square roots (transformed value $=180/\pi\arcsin[\sqrt{(\%/100)}]$) to normalize them and stabilize variances throughout the data range, and subjected to analysis of variance using SPSS software, after which residual plots

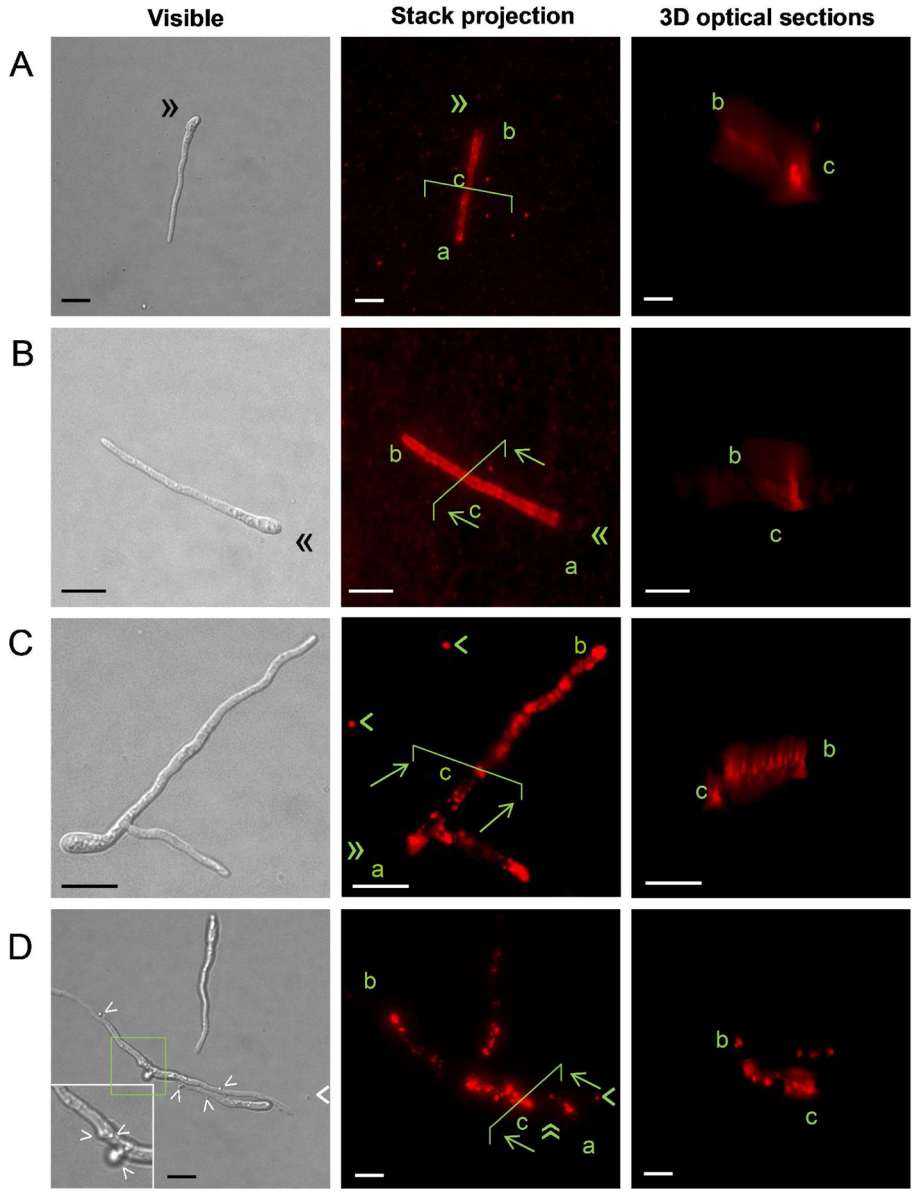

Figure 1. Dynamics of MPA-QDs in a suspension of growing *F. oxysporum*. Pictures represent visible and confocal micrographs of overview images (stack projections) and the transverse optical section obtained from the left image. Lower case letters indicate the orientation of the images for ease of understanding. The green hurdle in the overview images marks the plane of the section shown in the 3D images. *F. oxysporum* was incubated with MPA-QDs for (A) 10 min, (B) 3 h, and (C) 16 h. (D) Hyphal suspension was incubated with MPA-QDs for 16 h, filtered to remove any MPA-QDs from the medium, and incubated in new medium without MPA-QDs for an additional 4 h. Bars indicate 10 μm.

were inspected to confirm that the data conformed to normality. In addition, the Shapiro-Wilk test and Bartlett's test were performed to test the normality and homogeneity of variances, respectively. The significance of differences between means was determined by contrast analysis (Scheffe's).

3. RESULTS

3.1. MPA-QD and SiO_2-MNP Interaction with *F. oxysporum* Hyphal Cells. *MPA-QDs.* Confocal images of *F. oxysporum* suspensions incubated with MPA-QDs for 10 min showed their rapid attraction and internalization by the fungal hyphae, as shown in the stack projections and 3D optical sections (Figure 1A). This situation remained unchanged when samples were incubated for 3 h (Figure 1B). Up to this time, MPA-QDs appeared evenly distributed throughout the hyphae, but interestingly, the original conidia from which the hyphae grew did not attract them (double arrows Figure 1).

After 16 h of incubation with MPA-QDs, a different distribution pattern was observed. Thus, MPA-QDs were not homogeneously distributed but grouped in well-defined clusters in the hyphae (Figure 1C, stack projection). At this time, some MPA-QDs aggregates were also observed in the MM (Figure 1C, arrowhead, stack projection). When the fungal suspension was filtered to remove the MPA-QDs from the medium, and the mycelium was resuspended in new medium without MPA-QDs for 4 h, MPA-QDs were still observed in discrete aggregates inside the fungus although in a slightly lower number (Figure 1D stack projection). In addition MPA-QD aggregates were also detected on the fungal surface (Figure 1D, arrowheads in visible field) and in the medium (Figure 1D, arrowhead, visible and stack projection).

SiO_2-MNPs. Confocal images of *F. oxysporum* suspensions incubated with SiO_2-MNPs showed a distinct distribution to that of MPA-QDs. After 10 min of incubation, SiO_2-MNPs aggregates attached to the fungal hyphal surfaces (Figure 2A arrowhead at visible field and stack projection).

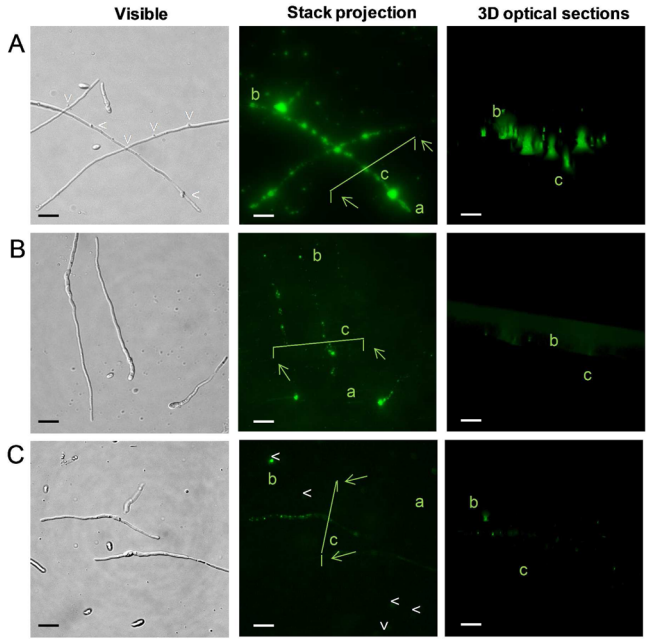

Figure 2. Dynamics of SiO_2-MNPs in a suspension of growing *F. oxysporum*. Pictures represent visible and confocal micrographs of overview images (stack projections) and the transverse optical section obtained. Lower case letters indicate the orientation of the images for ease of understanding. The green hurdle in the overview images marks the plane of the section shown in the 3D images. *F. oxysporum* was incubated with SiO_2-MNPs for (A) 10 min and (B) 16 h. (C) Hyphal suspension was incubated with SiO_2-MNPs for 16 h, filtered to remove any nanoparticles from the medium, and incubated in new medium without SiO_2-MNPs for an additional 4 h. Bars indicate 10 μm.

However, the nanoparticles did not penetrate the fungal hyphae because 3D optical sections showed a clear signal only for the largest aggregates.

Although the penetration of nonaggregated SiO_2-MNPs could not be inferred from the confocal images, it cannot be discarded. At 16 h of incubation, nanoparticle aggregates were still visible and attached on the hyphal surface, although they were smaller than those attached after a 10 min incubation, and no signal was observed in the 3D optical sections (Figure 2B). When the fungal suspensions were filtered to remove the SiO_2-MNPs from the medium, and the mycelium was resuspended in new medium without SiO_2-MNPs for 4 h, small aggregates were still observed on the fungal surface, whereas nonattached particles were also found in the medium (Figure 2C, arrow heads).

While MPA-QDs are highly fluorescent, the SiO_2-MNPs fluorescent signal is due to the AlexaFluor488-conjugated G protein adsorbed on the particle surface. To ensure that the fluorescent signal from the fungal hyphae effectively corresponded to the SiO_2-MNPs, we also performed TEM and STEM after the incubation of *F. oxysporum* with these nanoparticles. Transmission electron micrographs showed a range of small to medium aggregates corresponding to the SiO_2-MNPs attached to the fungal surface (Figure 3A).

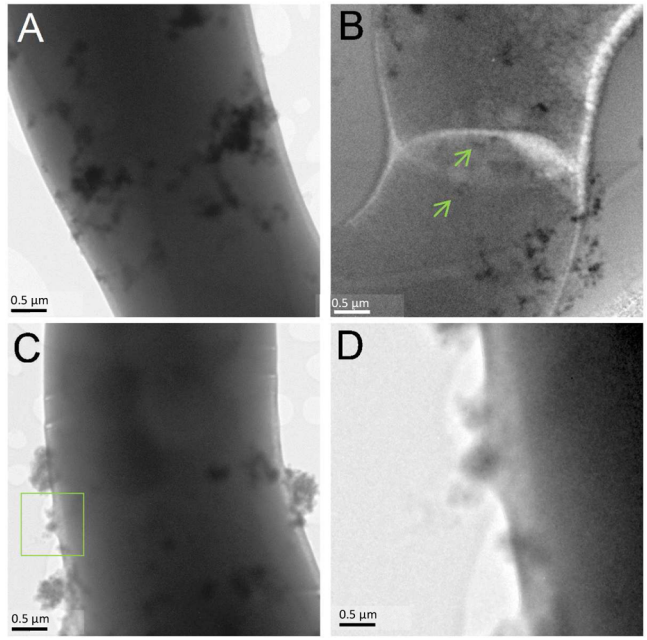

Figure 3. Transmision electron micrographs (BF-TEM) of *F. oxysporum* hyphae incubated with SiO_2-MNPs. *F. oxysporum* conidia were grown in minimum medium with SiO_2-MNPs for 16 h and then cryofixed by vitrification before bright-field TEM analysis. (A) Detail of a *F. oxysporum* hypha with SiO_2-MNPs adhered. (B) Observations of hyphal septum area and its interaction with SiO_2-MNPs. (C, D) SiO_2-MNPs adhered to the fungal hypha and detail of a small aggregate that moved through the membrane. Bars indicate 0.5 μm.

The chemical nature of these aggregates was confirmed by EDS spectra and STEM-HAADF images. This technique is highly sensitive to variations in the atomic number of each atom present in the material, yielding a Z-contrast image, in which it is easy to identify SiO_2-MNPs interacting with fungal cells. In addition, EDS confirmed that the aggregates (Figure 4A) corresponded to the iron in the magnetic core and the silicon in the nanoparticle coating (Figure 4B–D).

TEM images revealed that most nanoparticles were clearly on the surface, outside the cells (Figure 3B). However, detailed observations near to the septum area and focal series of STEM-HAADF images, which present a smaller focal depth than TEM, suggested that individual SiO_2-MNPs could enter the fungal cells. This was also observed by TEM, since some of the smallest aggregates moved through the fungal cell wall (Figure 3C, D).

Recognition of the SiO_2-MNPs by the fungal hyphae was confirmed through magnetic separation assays followed by turbidity measurements. When fungal conidia were grown in the absence of SiO_2-MNPs, they remained in solution after the application of the magnetic field, as indicated by the turbidity (or relative absorbance) of the suspension shown in Figure 5A (open circles). The small decrease in the turbidity of these samples could be related to the slight precipitation effect that follows vortex stirring, a process necessary for sample homogenization prior to absorbance measurements. Interestingly, when fungal conidia were incubated in the presence of the SiO_2-MNPs for 16 h, filtered, and then resuspended in new medium without nanoparticles, they were attracted by the magnet as early as 1 min after application of the magnetic field. Thus, the turbidity of the medium was reduced dramatically (Figure 5A), confirming attachment of the nanoparticles to the

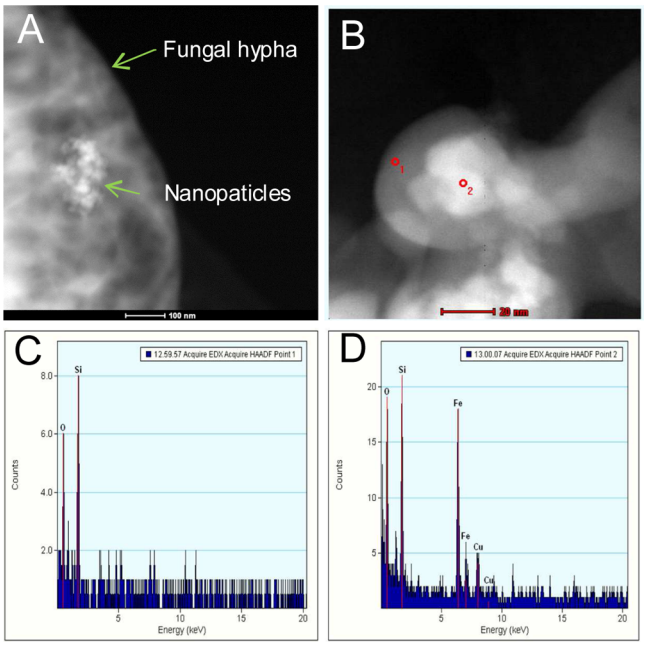

Figure 4. Energy-dispersive X-ray spectroscopy (EDS) of high-angle annular dark-field (HAADF) scanning transmission electron microscopy (STEM). (A) Fungal hypha with a SiO_2-MNPs aggregate adhered. (B) Detail of the SiO_2-MNPs showing the nucleus (o2) and the silica shell (o1). (C, D) Spectra of the corresponding o1 and o2 area confirming that dark aggregates corresponded to the SiO_2-MNPs. Bars indicate 100 and 20 nm in panels A and B, respectively.

hyphae. During the following 4 min, the turbidity decreased further but the highest reduction with respect to the control samples (without magnet application) was observed during the first minute. We also tested whether functionalization of the SiO_2-MNPs with Protein G (PG) influences the fungus-nanoparticle interaction. Incubation of conidia with the PG-functionalized SiO_2-MNPs caused a small delay in particle movement toward the magnet. Nevertheless, after 5 min, the amount of particles in the proximity of the magnet and therefore the turbidity of the medium were similar to those of nonfunctionalized nanoparticles.

In a second "short-term" experiment, conidia were grown in the absence of SiO_2-MNPs, then incubated with PG-functionalized SiO_2-MNPs for 5 s, 15 min, and 30 min. They were then filtered, resuspended in new medium, and subjected to the magnetic field of the magnetic separation rack. Incubation of fungal conidia with SiO_2-MNPs for as short as 5 s, drastically reduced the turbidity of the medium when subjected to the magnetic field (Figure 5B). This observation confirmed the high affinity and rapid attraction of the nanoparticles for the fungal hyphae.

3.2. MPA-QDs and SiO_2-MNPs Toxicity on *F. oxysporum* Hyphal Cells. Assessment of the growth of *F. oxysporum* conidia when incubated with a range of concentrations of MPA-QDs showed that only the highest concentration, 500 nM, several fold over the normal concentration used for biological applications, had a negative effect on germination and hyphal growth. This concentration reduced the percentage of long hyphae and the average area of hyphae to an even greater extent than the slight heat shock treatment used as a positive control (Table 1). Analysis of SiO_2-MNPs assay showed a reduction in the percentage of germination at 100 μg mL^{-1},whereas the heat shock treatment reduced both the percentage of germination and hyphal area, as in the QD assay (Table 1).

Cells treated with 3,3′-diaminobenzidine (DAB) in the absence of oxidative stress did not present the typical brown precipitate caused by the presence of hydrogen peroxide (H_2O_2), which is indicative of oxidative stress (Figure 6A). Cells treated for 20 min at 50 °C with subsequent addition of DAB showed a brownish color (Figure 6A).

Indeed, the DAB assay revealed a high generation of H_2O_2 in fungal suspensions subjected to the heat shock treatment, with approximately 80% of conidia showing brown staining (Figure 6B). Incubation of the fungal conidia with the MPA-QDs or the SiO_2-MNPs did not increase H_2O_2 production within fungal hyphae, as inferred by the absence of staining (Figure 6B). Interestingly, incubation of hyphal cells with QDs slightly but significantly reduced the level of H_2O_2 with respect to that of conidia incubated in the absence of MPA-QDs.

After heating the *F. oxysporum* conidial suspensions for 20 min at 50 °C, nearly 100% of the hyphae exhibited dark blue

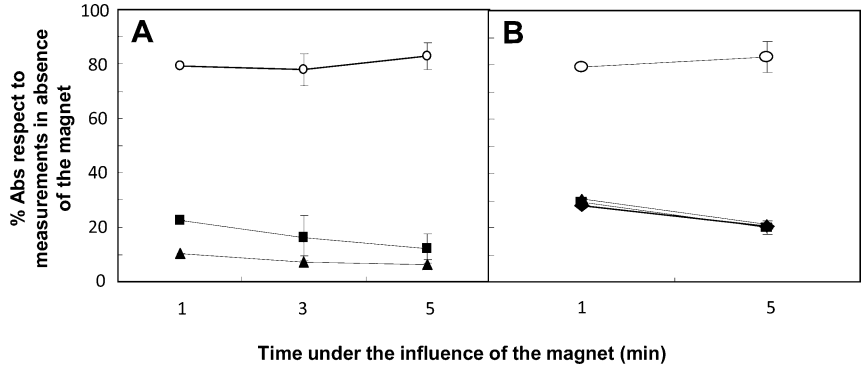

Figure 5. Effect of a magnetic field on fungal hyphae incubated in the presence of SiO_2-MNPs. The absorbance at 600 nm (A_{600}) of a fungal conidial suspension incubated with or without the SiO_2-MNPs was measured after placing the suspension in a magnetic separation rack, and percentages with respect to absorbance in the absence of the magnet (control) were calculated. (A) Fungal conidia were grown for 16 h in the absence (open circles) or presence of 200 μg mL^{-1} SiO_2-MNPs functionalized with G Protein (solid square) or nonfunctionalized (solid triangles) and then subjected to the magnetic field. (B) Fungal conidia were grown for 16 h in the absence of SiO_2-MNPs, then incubated for 5 s (solid squares), 15 min (solid triangles) and 30 min (solid diamonds) with 200 μg mL^{-1} SiO_2-MNPs functionalized with a G Protein, and finally subjected to the magnetic field. Open circles correspond to fungal suspensions incubated without nanoparticles. Data are the average of three independent replicates ± standard error.

dx.doi.org/10.1021/am501029g | ACS Appl. Mater. Interfaces 2014, 6, 9100−9110

Table 1. Effect of Nanoparticles on Colony Growth[a]

	% germination	% long hyphae	area ($mm^2 \times 100$)
	MPA-QDs		
0 nM	86.7^{ns}	30.0	51.41
10 nM	84.3 ^{ns}	27.3 ^{ns}	58.59^{ns}
50 nM	85.7 ^{ns}	34.0 ^{ns}	53.70^{ns}
100 nM	87.3 ^{ns}	32.0 ^{ns}	51.57^{ns}
500 nM	20.0***	15.4*	19.14***
heat	73.3**	21.3^{ns}	34.02**
l.s.d.	10.5	14.5	10.52
	SiO_2-MNPs		
0 μg/mL	86.7	30.0	124.27
25 μg/mL	84.3^{ns}	28.0^{ns}	114.35^{ns}
50 μg/mL	78.3^{ns}	25.7^{ns}	114.12^{ns}
100 μg/mL	73.0*	24.3^{ns}	106.88^{ns}
500 μg/mL	77.0^{ns}	21.3^{ns}	127.86^{ns}
heat	73.3**	21.3^{ns}	96.65*
l.s.d.	11.5	6.3	22.91

[a]*, **, and *** indicate significant differences with respect to the control without nanoparticles at $P < 0.05$, 0.01, and 0.001 respectively. ns indicates no significant differences.

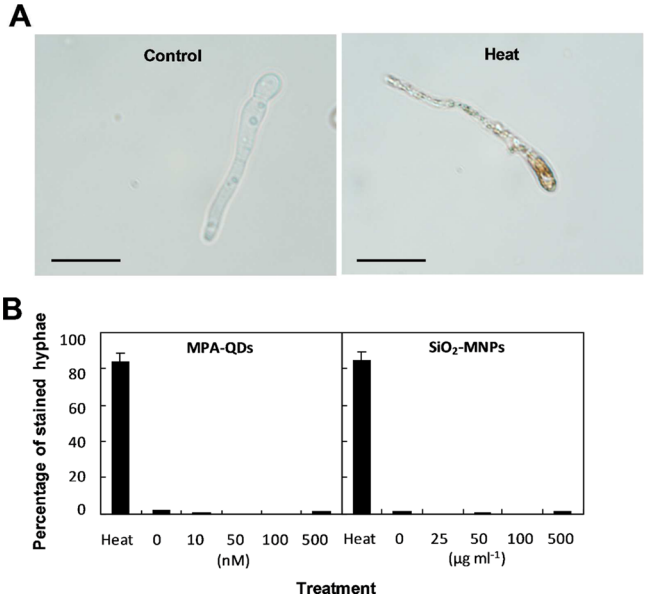

Figure 6. Assessment of H_2O_2 generation of *F. oxysporum* following treatment with MPA-QDs and SiO_2-MNPs. (A) Optical microscopy images of negative control incubated in the absence of MPA-QDs and SiO_2-MNPs. and positive control treated with heat following application of DAB stain. Bars indicate 20 μm. (B) Quantification of positive DAB hyphae following incubation with a range of concentrations of MPA-QDs and SiO_2-MNPs.

formazan spots (Figure 7A). These deposits indicated that superoxide anion ($O_2^{-\bullet}$) was produced by these structures at a higher rate than its detoxification in response to the heat stress, since no spots were seen in the controls (Figure 7A).

Although very low levels of $O_2^{-\bullet}$ generation were observed in controls grown in the absence of MPA-QDs, fungal suspensions incubated with these particles, at any of the concentrations tested, induced $O_2^{-\bullet}$ generation similar to that observed in the heat- treated samples (Figure 7B). However, fungal suspensions incubated with the SiO_2-MNPs showed a distinct behavior, since only the concentration of 50 μg mL^{-1} significantly increased the $O_2^{-\bullet}$ with respect to the controls

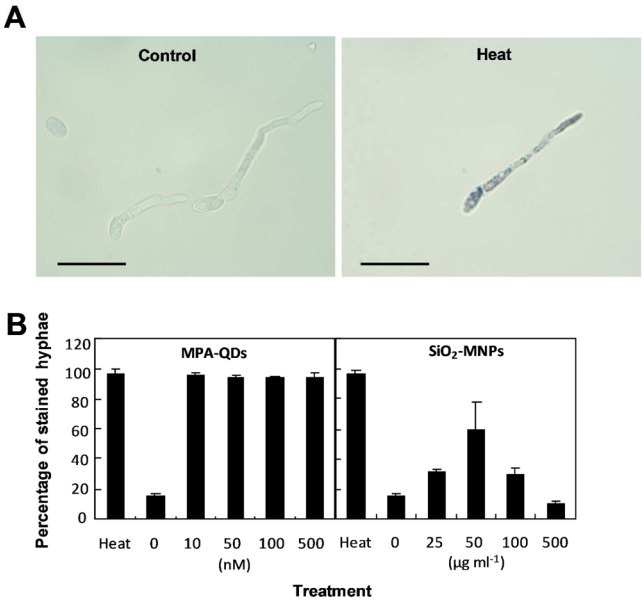

Figure 7. Assessment of $O_2^{-\bullet}$ generation on *F. oxysporum* following treatment with MPA-QDs and SiO_2-MNPs. (A) Optical microscopy images of negative control incubated in the absence of MPA-QDs and SiO_2-MNPs and positive control treated with heat following application of NBT stain. Bars indicate 20 μm. (B) Quantification of positive NBT hyphae following incubation with a range of concentrations of MPA-QDs and SiO_2-MNPs.

incubated in the absence of SiO_2-MNPs and this occurred to a significantly lower extent than in the heat-treated samples.

When treated with 2′,7′-dichlorodihydrofluorescein diacetate (H_2DCFDA), control hyphae showed a basal-level fluorescent signal, as previously reported (Figure 8A[31]). In heat-treated samples, the H_2DCFDA signal was significantly increased (Figure 8A), thus showing a response in terms of ROS accumulation.

Interestingly, while concentrations of 10 and 50 μg mL^{-1} of MPA-QDs induced similar fluorescence than controls, higher concentrations significantly reduced this fluorescence, thereby indicating lower oxidative stress (Figure 8B). No effect of SiO_2-MNPs on H_2DCFDA fluorescence was observed with any of the concentrations tested (Figure 8B).

Dead fungal cells treated with Evans Blue presented a typical blue coloration, which was not observed in living hyphae (Figure 9A). Fungal cell viability assays showed that there was a negligible impact of the type and concentration of nanoparticles on cell viability, especially when compared with the impact of the heat stress on positive controls (Figure 9B). Only the highest concentration of MPA-QDs and the 25 μg/mL of SiO_2-MNPs lead to a slightly higher percentage of dead hyphae than the reference. However, in these cases, the observed variation was not higher than 4% of dead cells. No significant differences were found when incubated the fungus with these nanomaterials for up to 48 h (see the Supporting Information).

4. DISCUSSION

One of the major challenges in pathology is the early and accurate detection of diseases. A number of new, highly sensitive, diagnostic nanotechnology-based platforms have recently been developed to detect biomolecules and cells. These could allow the early detection of diseases or could provide valuable insight into biology at the system levels.[32] In

dx.doi.org/10.1021/am501029g | ACS Appl. Mater. Interfaces 2014, 6, 9100−9110

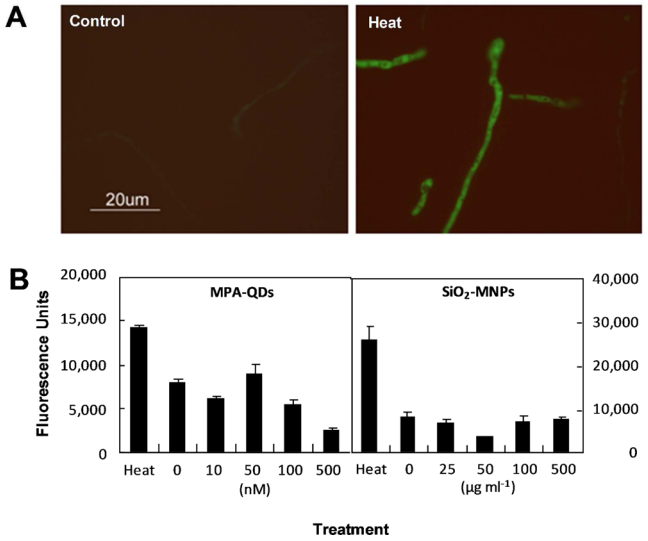

Figure 8. Assessment of cellular stress on *F. oxysporum* following treatment with MPA-QDs and SiO_2-MNPs. (A) Microscopy images of negative control incubated in the absence of MPA-QDs and SiO_2-MNPs and positive control treated with heat following application of H_2DCFDA stain. Bars indicate 20 μm. (B) Quantification of H_2DCFDA fluorescence of *F. oxysporum* hyphae following incubation with a range of concentrations of MPA-QDs and SiO_2-MNPs.

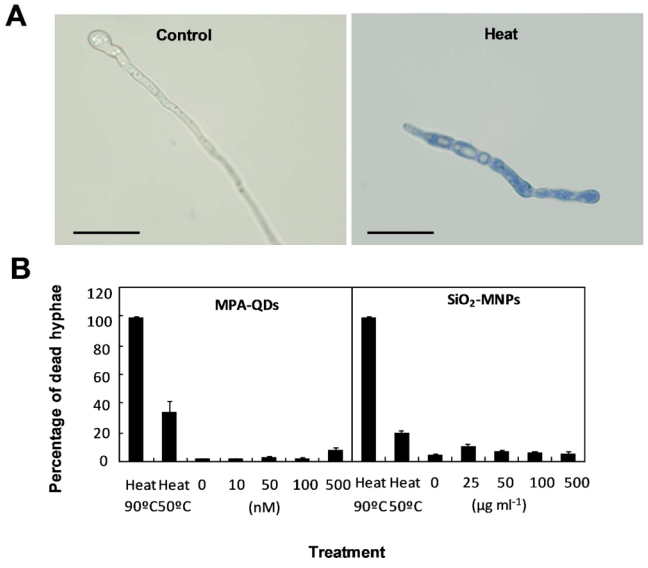

Figure 9. Assessment of cell viability of *F. oxysporum* following treatment with MPA-QDs and SiO_2-MNPs. (A) Optical microscopy of negative control incubated in the absence of MPA-QDs and SiO_2-MNPs and positive control treated with heat following application of Evans Blue stain. Bars indicate 20 μm. (B) Quantification of positive Evans Blue hyphae after incubation with a range of concentrations of MPA-QDs and SiO_2-MNPs.

addition, nanomaterials are attracting attention as potential drug delivery carriers[33] and hence as novel tools for the direct control of diseases. Here, we assessed two distinct types of nanosized materials as potential tools for the detection and/or control of *F. oxysporum*, one of the main constraints for many crops[34] and an opportunistic human pathogen.[2]

The choice of QDs and superparamagnetic nanoparticles in this study arose from their wide use for biological and medical research in recent years and because they have different physical properties but are similarly robust, versatile, and possess a high potential for high-throughput biosensing platforms.[32,35] QDs are easily detected because of their unusually intense and photostable fluorescence, thus avoiding the shortcomings—such as autofluorescence and photobleaching—of organic fluorophores. Thus, QDs are a highly suitable option when superior performance is required to achieve lower limits of detection, more quantitative results, greater sample photostability, or higher levels of multiplexability.[35] On the other hand, biological samples exhibit virtually no magnetic background and thus the use of magnetic nanoparticles allows highly sensitive measurements in turbid or otherwise visually obscured samples without further processing. Indeed numerous methods including magnetization measurements, such as those performed by means of high-sensitivity SQUID magnetometers,[36,37] magnetoresistive sensors,[14] Hall sensors,[38] and approaches based on magnetic resonance[39] have been successfully developed to sense biomolecules using magnetic nanoparticles.

Imaging of the interaction of *F. oxysporum* with the two types of nanomaterials by means of confocal microscopy showed distinct behaviors between MPA-QDs and SiO_2-MNPs. Both showed high interaction with the fungal cells; however, while MPA-QDs readily penetrated the fungal hyphae, most of the SiO_2-MNPs remained attached to the fungal cell wall surface. Recent investigations into the nature of the relationship between cellular uptake and physicochemical properties of nanosized objects indicate that their entry into cells is dependent on many factors, such as their size, charge, hydrophobicity, or even ligand arrangement. Thus, in the present study, size differences could have influenced the uptake since the MPA-QDs used were smaller than the SiO_2-MNPs (13.5 nm vs c.a. 100−150 nm diameter, respectively). In addition, MPA-QDs and SiO_2-MNPs showed distinct surface charges at the pH tested. Both of them were incubated together with the fungal conidia in liquid MM, which is characterized by a slightly acidic pH of 6, because this value is appropriate for *F. oxysporum* growth and it is also the xylem pH of plants from which the fungal spread occurs.[40] At this pH, δ-potential curves showed negative values (c.a. −35 mV) for MPA-QDs and positive values (of c.a. +25 mV) for SiO_2-MNPs.[22,24] Thus, both were in the range of moderate stability but with opposite charges.

Several studies have reported the interaction and uptake of various types of nanosized materials by animal and plant cells.[6,10,41−43] Indeed, recent studies have reported their potential for detection and control of human pathogenic bacteria and viruses.[44,45] However, to the best of our knowledge, no studies have addressed the interaction of such types of nanomaterials with hyphal cells, characterized by the presence of a fungal cell wall. Electron microscopy studies have reported that the cell wall structure of *F. oxysporum* consists of an outer layer with a high presence of proteins[46] enriched in glycoproteins,[47] and an inner layer composed mainly of chitin and β-1,3-glucan. Cell wall glycoproteins determine the antigenic and adhesive properties of the hyphae.[48] Particularly, one of the most abundant, glycosylphosphatidylinositol-modified (GPI) cell wall proteins, commonly named adhesins, have an N-terminal signal peptide and a C-terminal sequence containing a peptide for anchoring to a preformed GPI site that mediates the adhesion to organic and inorganic surfaces.[49] This site might also mediate the adhesion of the larger SiO_2-MNPs. In addition, because the glycoproteins are negatively charged,

dx.doi.org/10.1021/am501029g | ACS Appl. Mater. Interfaces 2014, 6, 9100−9110

positively charged SiO_2-MNPs would be attracted by electrostatic interactions.[10] Neutral or negatively charged QDs have been reported to be more weakly bound to glycoproteins; however, it was also shown that QDs and nanoparticles with a negative charge can be massively internalized when their concentration is sufficient.[6,50] Therefore, since both MPA-QDS and SiO_2-MNPs interacted with the fungal hyphae, the massive internalization of QDs could be explained by their small diameter. Indeed, the larger size of aggregates of SiO_2-MNPs formed on the hyphae surface, which made them visible in the confocal and even visible field, may hinder their uptake, similarly to the slight aggregation in the media at high nanoparticle concentration. Interestingly, fewer aggregates were observed following longer incubation periods. This finding could be attributed to the slight acidification of the incubation medium during *F. oxysporum* growth.[51] This acidification might increase the δ-potential and improve the stability of the SiO_2-MNPs. It has been suggested that, given their small size, QDs could cross the plasma membrane mainly through pinocytosis, a distinct endocytotic mechanism, chiefly responsible for the uptake of cell nutrients and other small particles.[10] However, the contribution of the specific endocytic clathrin/caveolae-dependent/independent route remains to be clarified.

Focusing on the internalized MPA-QDs, their distribution pattern dramatically changed from an even and uniform distribution in the short term incubations (10 min and 3 h), where they were observed throughout the cytoplasm, to a grouping in large clusters within the hyphal cells at longer incubation time (16 h). This change in distribution has been previously reported and suggested to be due to nanoparticle processing and compartmentalization.[9] Many studies have revealed the preferential localization of QDs in lysosomes, a common terminus of several endocytic pathways. During uptake, QDs are internalized into endocytic vesicles, which fuse with early endosomes and lysosomes.[52,53] Early endosomes that contain QDs have also been observed to traffic back to the plasma membrane in a process which may contribute to QD exocytosis.[50] Our data support the notion of QD back trafficking since, after filtration of the incubation medium to remove them and resuspension of the mycelium in new medium, QD aggregates were detected on the surface of the fungal cell wall and also in the medium. Although it has been postulated that P-glycoprotein transporters are involved in QD removal,[54] there is no consensus as yet on which of the specific processes leads to QD release and on the possible involvement of exocytic mediators.

Of the few studies on nanomaterials devoted to fungi, these have focused mainly on the potential of fungi to synthesize the nanomaterials.[55] Indeed, extracellular biosynthesis of silver nanoparticles from ionic silver occurs in *F.* oxysporum.[56] There are limited studies on the toxicity of metal nanoparticles, and these have reported only a direct toxic effect of silver on the fungal growth and viability of *Candida* spp, *F. culmorum* and *Trychophyton mentagrophytes* comparable to that of ionic silver.[57,58] Here we assessed the toxicity of MPA-QDs and SiO_2-MNPs on *F. oxysporum* over a range of concentrations using cell-based toxicity tests. These tests allow the setup of high-throughput systems for rapid and cost-effective screening of hazards, while targeting the biological responses under highly controlled conditions.[59] Our assessment included the evaluation of fungal germination and growth, the production and accumulation of ROS, particularly H_2O_2 and $O_2^{-\bullet}$, and fungal viability. Our data showed that MPA-QDs and SiO_2-MNPs exerted distinct effects on *F. oxysporum* and that they also showed a concentration-dependent effect. Differences may arise from the distinct uptake previously described, and also from the diverse nature of the materials and their stabilizing shells.

Only the highest MPA-QD concentration, which greatly exceeded the concentrations commonly used in biological applications, showed an effect on conidial germination and hyphal growth. In contrast, intermediate concentrations of SiO_2-MNPs slightly but significantly reduced conidial germination. This was not seen at higher concentrations probably because of the aggregate formation observed, which could limit the effect of the SiO_2-MNPs. Indeed, the large surface area per mass compared with larger-sized particles is what makes SiO_2-MNPs more reactive biologically.[60] Thus, aggregate formation would render SiO_2-MNPs less reactive. This observation has raised the importance of testing a range of concentrations in toxicity assays, paying special attention to the possible concentration-induced aggregation effect.[61] This effect of the SiO_2-MNPs was also observed in the $O_2^{-\bullet}$ and cell viability assessments. Surprisingly, H_2O_2 production, which can damage various molecular targets, including DNA, protein, and lipids, was not observed under the conditions assayed with MPA-QDs and SiO_2-MNPs. Indeed, a significant decrease in H_2O_2 production was detected after several of the treatments. This observation might be attributable to the antioxidant properties of some nanosized materials, such as fullerenes, which may prevent lipid peroxidation induced by superoxide and hydroxyl radicals.[62] In addition, Gao et al.[63] reported that bare magnetic iron oxide nanoparticles exhibit peroxidase-like activity, which reduces the amount of H_2O_2 present in the cells. Our data support a peroxidase-like activity for both MPA-QDs and SiO_2-MNPs, because although a decrease in H_2O_2 was observed, $O_2^{-\bullet}$ generation was increased at all the QD concentrations tested and at intermediate concentrations of SiO_2-MNPs. The higher effect of MPA-QDs on $O_2^{-\bullet}$ generation compared with SiO_2-MNPs could be due to the higher MPA-QD uptake and/or to a catalase-like activity, as described for iron oxide nanoparticles.[64]

5. CONCLUSION

In the work presented here, the interaction of two different inorganic nanoparticles, MPA-QDs and SiO_2-MNPs, with fungal cells has been addressed. To the best of our knowledge, the behavior of a fungal cell wall in the presence of such nanomaterials had not been undertaken to date. Both nanomaterials rapidly interacted with the fungal hypha labeling the presence of the pathogenic fungus, although they showed differential behavior with respect to internalization. Thus, whereas magnetic nanoparticles appeared to be in the cell surface, quantum dots were significantly uptaken by the fungal hyphae. In addition, different assays show a low toxicity profile for both types of nanomaterials to the fungus.

Overall, the internalization and toxicity studies showed that after an appropriate functionalization the MPA-QDs and SiO_2-MNPs might be applied for the rapid and sensitive detection of *F. oxysporum* and also for the control of this devastating pathogen. In both cases, in combination with a biomolecule able to target a desired *forma specialis*, they could act as inner- (in the case of MPA-QDs) or surface- (in the case of SiO_2-MNPs) fungus labels. In addition, the massive uptake of MPA-QDs by the fungal hypha and their low toxicity support their use as potential carriers that could be functionalized with drugs or with precise DNA/RNA sequences that are specific to the

different *F. oxysporum formae specialis* to be delivered inside the fungal cells. The capacity of SiO_2-MNPs to remain in sufficient amounts at the hyphal surface supports their use for magnetic separation applications and biosensing based on magnetic detection. This work opens a field for the development of new detection and control approaches based on nanotechnology.

■ ASSOCIATED CONTENT

Ⓢ Supporting Information

BF-TEM/TEM images, hydrodynamic diameter (DLS measurements) figures for both SiO_2-MNPs and MPA-QDots, Z-potential values, representative absorbance and fluorescence spectra of QDs, and assessment of cell viability of *F. oxysporum* following treatment with MPA-QDs and SiO2-MNPs over a 48 h time course are reported. This material is available free of charge via the Internet at http://pubs.acs.org.

■ AUTHOR INFORMATION

Corresponding Author

*E-mail: elena.prats@ias.csic.es. Tel: +34 957499291. Fax: +34 957499252.

Notes

The authors declare no competing financial interest.

■ ACKNOWLEDGMENTS

This work was supported by the Spanish Ministry of Science and Innovation, the EuroInvestigation program [EUI2008-00157], the European Regional and Social Development Funds, the ERC-Starting Grant-NANOPUZZLE, and AGR-253 funds. N.R. is supported by a Ramón y Cajal postdoctoral fellowship from the *Ministerio de Economia y Competitividad*. This study was also supported by the *Fundação para a Ciência e Tecnologia-Portugal* through a doctoral grant to A.S.M. (SFRH/BD/40303/2007) and by grant Pest-OE/EQB/LA0004/2011. We also thank B. Espejo for technical assistance.

■ REFERENCES

(1) Di Pietro, A.; Madrid, M. P.; Caracuel, Z.; Delgado-Jarana, J.; Roncero, M. I. G. *Fusarium oxysporum*: Exploring the Molecular Arsenal of a Vascular Wilt Fungus. *Mol. Plant Pathol.* **2003**, *4*, 315−325.

(2) Boutati, E. I.; Anaissie, E. J. *Fusarium*, a Significant Emerging Pathogen in Patients with Hematologic Malignancy: Ten Years' Experience at a Cancer Center and Implications for Management. *Blood* **1997**, *90*, 999−1008.

(3) Amini, J.; Sidovich, D. The Effects of Fungicides on *Fusarium oxysporum* f.sp. *lycopersici* Associated with Fusarium Wilt of Tomato. *J. Plant Prot. Res.* **2010**, *50*, 172−178.

(4) Marois, J. J.; Mitchell, D. J. Effects of Fumigation and Fungal Antagonists on the Relationships of Inoculum Density to Infection Incidence and Disease Severity in Fusarium Crown Rot of Tomato. *Phytopathology* **1981**, *71*, 167−170.

(5) Jiménez-Fernández, D.; Montes-Borrego, M.; Navas-Cortés, J. A.; Jiménez-Díaz, R. M.; Landa, B. Identification and Quantification of *Fusarium oxysporum* in Planta and Soil by Means of an Improved Specific and Quantitative PCR Assay. *Appl. Soil Ecol.* **2010**, *46*, 372−382.

(6) Moros, M.; Hernaez, B.; Garet, E.; Dias, J. T.; Saez, B.; Grazu, V.; Gonzalez-Fernandez, A.; Alonso, C.; de la Fuente, J. M. Monosaccharides *versus* PEG-Functionalized NPs: Influence in the Cellular Uptake. *ACS Nano* **2012**, *6*, 1565−1577.

(7) Pankhurst, Q. A.; Connolly, J.; Jones, S. K.; Dobson, J. Applications of Magnetic Nanoparticles in Biomedicine. *J. Phys. D: Appl. Phys.* **2003**, *36*, 167−181.

(8) Jain, K. K. Nanotechnology in Clinical Laboratory Diagnostics. *Clin. Chim. Acta* **2005**, *358*, 37−54.

(9) Mahmoudi, M.; Sant, S.; Wang, B.; Laurent, S.; Sen, T. Superparamagnetic Iron Oxide Nanoparticles (SPIONs): Development, Surface Modification and Applications in Chemotherapy. *Adv. Drug Delivery Rev.* **2011**, *63*, 24−46.

(10) Al-Hajaj, N. A.; Moquin, A.; Neibert, K. D.; Soliman, G. M.; Winnik, F. M.; Maysinger, D. Short Ligands Affect Modes of QD Uptake and Elimination in Human Cells. *ACS Nano* **2011**, *5*, 4909−4918.

(11) Fernández-Suárez, M.; Ting, A. Y. Fluorescent Probes for Super-Resolution Imaging in Living Cells. *Nat. Rev. Mol. Cell Biol.* **2008**, *9*, 929−943.

(12) Ferrari, M. Cancer Nanotechnology: Opportunities and Challenges. *Nat. Rev. Cancer* **2005**, *5*, 161−171.

(13) Laurent, S.; Forge, D.; Port, M.; Roch, A.; Robic, C.; Elst, L. V.; Muller, R. N. Magnetic Iron Oxide Nanoparticles: Synthesis, Stabilization, Vectorization, Physicochemical Characterizations, and Biological Applications. *Chem. Rev.* **2008**, *108*, 2064−2110.

(14) Serrate, D.; de Teresa, J. M.; Marquina, C.; Marzo, J.; Saurel, D.; Cardoso, F. A.; Cardoso, S.; Freitas, P. P.; Ibarra, M. R. Quantitative Biomolecular Sensing Station Based on Magnetoresistive Patterned Arrays. *Biosens. Bioelectron.* **2012**, *35*, 3495−3498.

(15) Xu, P.; Zeng, G. M.; Huang, D. L.; Feng, C. L.; Hu, S.; Zhao, M. H.; Lai, C.; Wei, Z.; Huang, C.; Xie, G. X.; Liu, Z. F. Use of Iron Oxide Nanomaterials in Wastewater Treatment: A review. *Sci. Total Environ.* **2012**, *424*, 1−10.

(16) Gong, J. L.; Wang, B.; Zeng, J. M.; Yang, C. P.; Niu, C. G.; Niu, Q. Y.; Zhou, W. J.; Liang, Y. Removal of Cationic Dyes From Aqueous Solution Using Magnetic Multi-Wall Carbon Nanotube Nanocomposite as Adsorbent. *J. Hazard. Mater.* **2009**, *164*, 1517−1522.

(17) Validov, S. Z.; Kamilova, F. D.; Lugtenberg, B. J. J. Monitoring of Pathogenic and Non-Pathogenic *Fusarium oxysporum* Strains During Tomato Plant Infection. *Microb. Biotechnol.* **2011**, *4*, 82−88.

(18) Wu, W.; He, Q.; Jiang, C. Magnetic Iron Oxide Nanoparticles: Synthesis and Surface Functionalization Strategies. *Nanoscale Res. Lett.* **2008**, *3*, 397−415.

(19) Di Pietro, A.; Roncero, M. I. G. Cloning, Expression, and Role in Pathogenicity of *pg1* Encoding the Major Extracellular Endopolygalacturonase of the Vascular Wilt Pathogen *Fusarium oxysporum*. *Mol. Plant-Microbe Interact.* **1998**, *11*, 91−98.

(20) Puhalla, J. E. Classification of Strains of *Fusarium oxysporum* on the Basis of Vegetative Compatibility. *Can. J. Bot.* **1985**, *63*, 179−183.

(21) Miguel, A.; Maycock, C.; Oliva, A. Synthesis and Functionalization of CdSe/ZnS QDs Using the Successive Ion Layer Adsorption Reaction and Mercaptopropionic Acid Phase Transfer Methods. *Methods Mol. Biol. (N. Y.)* **2012**, *906* (Part 2), 143−155.

(22) Santos, A. R.; Miguel, A. S.; Tomaz, L.; Malho, R.; Maycock, C.; Vaz Patto, M. C.; Fevereiro, P.; Oliva, A. The Impact of CdSe/ZnS Quantum Dots in Cells of *Medicago sativa* in Suspension Culture. *J. Nanobiotechnol.* **2010**, *8*, 24−38.

(23) Gill, R.; Freeman, R.; Xu, J.; Willner, I.; Winograd, S.; Shweky, I.; Banin, U. Probing Biocatalytic Transformations with CdSe−ZnS QDs. *J. Am. Chem. Soc.* **2006**, *128*, 15376−15377.

(24) De Matteis, L.; Custardoy, L.; Fernández-Pacheco, R.; Magén, C.; de la Fuente, J. M.; Marquina, C.; Ibarra, M. R. Ultrathin MgO Coating of Superparamagnetic Magnetite Nanoparticles by Combined Coprecipitation and Sol-Gel Synthesis. *Chem. Mater.* **2012**, *24*, 451−456.

(25) Arenal, R.; De Matteis, L.; Custardoy, L.; Mayoral, L.; Grazu, V.; de la Fuente, J. M.; Marquina, C.; Ibarra, M. R. Spatially-Resolved EELS Analysis of Antibody Distribution on Bio-Functionalized Magnetic Nanoparticles. *ACS Nano* **2013**, *7*, 4006−4013.

(26) Thordal-Christensen, H.; Zhang, Z. G.; Wei, Y. D.; Collinge, D. B. Subcellular Localization of H_2O_2 in Plants. H_2O_2 Accumulation in Papillae and Hypersensitive Response During the Barley-Powdery Mildew Interaction. *Plant J.* **1997**, *11*, 1187−1194.

(27) Fryer, M. J.; Oxborough, K.; Mullineaux, P. M.; Baker, N. R. Imaging of Photo-Oxidative Stress Responses in Leaves. *J. Exp. Bot.* **2002**, *53*, 1249−1254.
(28) Ortega-Villasante, C.; Rellan-Alvarez, R.; Del Campo, F. F.; Carpena-Ruiz, R. O.; Hernandez, L. E. Cellular Damage Induced by Cadmium and Mercury in *Medicago sativa*. *J. Exp. Bot.* **2005**, *56*, 2239−2251.
(29) Prats, E.; Mur, L. A. J.; Sanderson, R.; Carver, T. L. W. Nitric Oxide Contributes Both to Papilla-Based Resistance and the Hypersensitive Response in Barley Attacked by *Blumeria graminis* f. sp. *hordei*. *Mol. Plant Pathol.* **2005**, *6*, 65−78.
(30) Baker, C. J.; Mock, N. M. An Improved Method for Monitoring Cell Death in Cell Suspension and Leaf Disc Assays Using Evans Blue. *Plant Cell, Tissue Organ Cult.* **1994**, *39*, 7−12.
(31) Ashtamker, C.; Kiss, V.; Sagi, M.; Davydov, O.; Fluhr, R. Diverse Subcellular Locations of Cryptogein-Induced Reactive Oxygen Species Production in Tobacco Bright Yellow-2 Cells. *Plant Physiol.* **2007**, *143*, 1817−1826.
(32) Haun, J. B.; Yoon, T.-J.; Lee, H.; Weissleder, R. Magnetic Nanoparticle Biosensors. *Wiley Interdiscip. Rev.: Nanomed. Nanobiotechnol.* **2010**, *2*, 291−304.
(33) Pérez-de-Luque, A.; Hermosín, C. Nanotechnology and Its Use in Agriculture. In *Bio-Nanotechnology: A Revolution in Food, Biomedical and Health Sciences*; Bagchi, D., Bagchi, M., Moriyama, H., Shahidi, F., Eds.; Wiley-Blackwell: Hoboken, NJ, 2013; pp 383−398.
(34) Mandeel, Q. A. Influence of Plant Root Exudates, Germ Tube Orientation and Passive Conidia Transport on Biological Control of Fusarium Wilt by Strains of Nonpathogenic *Fusarium oxysporum*. *Mycopathologia* **2006**, *161*, 173−182.
(35) Ghasemi, Y.; Peymani, P.; Afifi, S. Quantum Dot: Magic Nanoparticle For Imaging, Detection and Targeting. *Acta Bio Med. Atenei Parmensis* **2009**, *80*, 156−65.
(36) Hao, L.; Cox, D.; See, P.; Gallop, J.; Kazakova, O. Magnetic Nanoparticle Detection Using Nano-SQUID Sensors. *J. Phys. D: Appl. Phys.* **2010**, *43*, 4004−4009.
(37) Kotitz, R.; Matz, H.; Trahms, L.; Koch, H.; Weitschies, W.; Rheinlander, T.; Semmler, W.; Bunte, T. SQUID Based Remanence Measurements for Immunoassays. *IEEE Trans. Appl. Supercond.* **1997**, *7*, 3678−3681.
(38) Aytur, T.; Foley, J.; Anwar, M.; Boser, B.; Harris, E.; Beatty, P. R. A Novel Magnetic Bead Bioassay Platform Using a Microchip-Based Sensor for Infectious Disease Diagnosis. *J. Immunol. Methods* **2006**, *314*, 21−29.
(39) Lee, H.; Sun, E.; Ham, D.; Weissleder, R. Chip-NMR Biosensor for Detection and Molecular Analysis of Cells. *Nat. Med.* **2008**, *14*, 869−874.
(40) Wilkinson, S.; Corlett, J. E.; Oger, L.; Davies, W. J. Effects of Xylem pH on Transpiration from Wild-Type and Flacca Tomato Leaves. A Vital Role for Abscisic Acid in Preventing Excessive Water Loss Even from Well-Watered Plants. *Plant Physiol.* **1998**, *117*, 703−709.
(41) Corredor, E.; Risueño, M.; Testillano, P. S. Carbon-Iron Magnetic Nanoparticles for Agronomic Use in Plants, Promising but Still a Long Way to Go. *Plant Signaling Behav.* **2010**, *5*, 1295−1297.
(42) Corredor, E.; Testillano, P. S.; Coronado, M.; González-Melendi, P.; Fernández-Pacheco, R.; Marquina, C.; Ibarra, M. R.; de la Fuente, J. M.; Rubiales, D.; Pérez-de-Luque, A.; Risueño, M. Penetration and Transport of Nanoparticles in Living Plants as a Tool for Directed Delivery: in Situ Detection into Plant Cells. *BMC Plant Biol.* **2009**, *9*, 45.
(43) Zhang, L. W.; Monteiro-Riviere, N. A. Mechanisms of Quantum Dot Nanoparticle Cellular Uptake. *Toxicol. Sci.* **2009**, *110*, 138−155.
(44) Luo, P. G.; Stutzenberger, F. J. Nanotechnology in the Detection and Control of Microorganisms. In *Advances in Applied Microbiology*, Laskin, A. L.; Sariaslani, S., Eds.; 2008; pp 145−181.
(45) Shinde, S. B.; Fernandes, C. B.; Patravale, V. B. Recent Trends in *In-Vitro* Nanodiagnostics for Detection of Pathogens. *J. Controlled Release* **2012**, *159*, 164−180.
(46) Klis, F. M. Cell Wall Assembly in Yeast. *Yeast* **1994**, *10*, 851−869.
(47) Schoffelmeer, E. A. M.; Klis, F. M.; Sietsma, J. H.; Cornelissen, B. J. C. The Cell Wall of *Fusarium oxysporum*. *Fungal Genet. Biol.* **1999**, *27*, 275−282.
(48) Wessels, J. G. H. Developmental Regulation of Fungal Cell-Wall Formation. *Annu. Rev. Phytopathol.* **1994**, *32*, 413−437.
(49) Li, F.; Svarovsky, M. J.; Karlsson, A. J.; Wagner, J. P.; Marchillo, K.; Oshel, P.; Andes, D.; Palecek, S. P. Eap1p, an Adhesin that Mediates *Candida albicans* Biofilm Formation *In-Vitro* and *In-Vivo*. *Eukaryotic Cell* **2007**, *6*, 931−939.
(50) Jiang, X.; Rocker, C.; Hafner, M.; Brandholt, S.; Dorlich, R. M.; Nienhaus, G. U. Endo- and Exocytosis of Zwitterionic Quantum Dot Nanoparticles by Live HeLa Cells. *ACS Nano* **2010**, *4*, 6787−6797.
(51) Brandao, R. L.; Castro, I. M.; Passos, J. B.; Nicoli, J. R.; Thevelein, J. M. Glucose-Induced Activation of the Plasma-Membrane H^+-ATP_{ase} in *Fusarium-oxysporum*. *J. Gen. Microbiol.* **1992**, *138*, 1579−1586.
(52) Behrendt, M.; Sandros, M. G.; McKinney, R. A.; McDonald, K.; Przybytkowski, E.; Tabrizian, M.; Maysinger, D. Imaging and Organelle Distribution of Fluorescent InGaP/ZnS Nanoparticles in Glial Cells. *Nanomedicine* **2009**, *4*, 747−761.
(53) Stern, S. T.; Zolnik, B. S.; McLeland, C. B.; Clogston, J.; Zheng, J.; McNeil, S. E. Induction of Autophagy in Porcine Kidney Cells by Quantum Dots: A Common Cellular Response to Nanomaterials? *Toxicol. Sci.* **2008**, *106*, 140−152.
(54) Orlowski, S.; Martin, S.; Escargueil, A. P-Glycoprotein and 'Lipid Rafts': Some Ambiguous Mutual Relationships: Floating on Them, Building Them or Meeting Them by Chance? *Cell. Mol. Life Sci.* **2006**, *63*, 1038−1059.
(55) Mandal, D.; Bolander, M. E.; Mukhopadhyay, D.; Sarkar, G.; Mukherjee, P. The Use of Microorganisms for the Formation of Metal Nanoparticles and Their Application. *Appl. Microbiol. Biotechnol.* **2006**, *69*, 485−492.
(56) Ahmad, A.; Mukherjee, P.; Senapati, S.; Mandal, D.; Khan, M. I.; Kumar, R.; Sastry, M. Extracellular Biosynthesis of Silver Nanoparticles Using the Fungus *Fusarium oxysporum*. *Colloids Surf., B* **2003**, *28*, 313−318.
(57) Kim, K.-J.; Sung, W. S.; Moon, S.-K.; Choi, J.-S.; Kim, J. G.; Lee, D. G. Antifungal Effect of Silver Nanoparticles on Dermatophytes. *J. Microbiol. Biotechnol.* **2008**, *18*, 1482−1484.
(58) Kim, K.-J.; Sung, W. S.; Suh, B. K.; Moon, S.-K.; Choi, J.-S.; Kim, J. G.; Lee, D. G. Antifungal Activity and Mode of Action of Silver Nano-Particles on *Candida albicans*. *Biometals* **2009**, *22*, 235−242.
(59) Jones, C. F.; Grainger, D. W. In Vitro Assessments of Nanomaterial Toxicity. *Adv. Drug Delivery Rev.* **2009**, *61*, 438−456.
(60) Oberdorster, G.; Oberdorster, E.; Oberdorster, J. Nanotoxicology: An Emerging Discipline Evolving from Studies of Ultrafine Particles. *Environ. Health Perspect.* **2005**, *113*, 823−839.
(61) Navarro, E.; Baun, A.; Behra, R.; Hartmann, N. B.; Filser, J.; Miao, A.-J.; Quigg, A.; Santschi, P. H.; Sigg, L. Environmental Behavior and Ecotoxicity of Engineered Nanoparticles to Algae, Plants, and Fungi. *Ecotoxicology* **2008**, *17*, 372−386.
(62) Wang, I. C.; Tai, L. A.; Lee, D. D.; Kanakamma, P. P.; Shen, C. K. F.; Luh, T. Y.; Cheng, C. H.; Hwang, K. C. C-60 and Water-Soluble Fullerene Derivatives as Antioxidants Against Radical-Initiated Lipid Peroxidation. *J. Med. Chem.* **1999**, *42*, 4614−4620.
(63) Gao, L.; Zhuang, J.; Nie, L.; Zhang, J.; Zhang, Y.; Gu, N.; Wang, T.; Feng, J.; Yang, D.; Perrett, S.; Yan, X. Intrinsic Peroxidase-Like Activity of Ferromagnetic Nanoparticles. *Nat. Nanotechnol.* **2007**, *2*, 577−583.
(64) Chen, Z.; Yin, J. J.; Zhou, Y.-T.; Zhang, Y.; Song, L.; Song, M.; Hu, S.; Gu, N. Dual Enzyme-Like Activities of Iron Oxide Nanoparticles and their Implication for Diminishing Cytotoxicity. *ACS Nano* **2012**, *6*, 4001−4012.
(65) Miguel, A. Quantum Dots: Synthesis, Functionalization and Bioconjugation for Biological Applications. *Ph.D. Thesis*, ITQB, Oeiras, Portugal, 2012; http://run.unl.pt/handle/10362/8594.